Photoluminescence in *m*-carborane-anthracene triads: a combined experimental and computational study

Mahdi Chaari,[a,b] Zsolt Kelemen,[a] José Giner Planas,[a] Francesc Teixidor,[a] Duane Choquesillo-Lazarte,[c] Abdelhamid Ben Salah,[b] Clara Viñas,[a] Rosario Núñez*[a]

[a] Institut de Ciència de Materials de Barcelona (ICMAB-CSIC), Campus U.A.B., 08193, Bellaterra, Barcelona, Spain.

[b] Laboratoire des Sciences des Matériaux et de l'Environnement, Faculté des Sciences de Sfax, Université de Sfax, B.P. 1171, 3000 Sfax, Tunisie.

[c] Laboratorio de Estudios Cristalográficos, IACT-CSIC, Avda. de las Palmeras 4 18100 – Armilla, Granada, Spain.

Corresponding Author: Dr. Rosario Núñez, Institut de Ciència de Materials de Barcelona, ICMAB-CSIC, Campus U.A.B., 08193 Bellaterra, Barcelona, Spain. Tel.: +34 93 580 1853. Fax: +34 93 580 5729. rosario@icmab.es

Abstract

New hybrids synthesized by linking two anthracenyl units to the $C_{cluster}$ atoms of a non- (**4**), a mono- (**5**) and a di-iodinated (**6**) *m*-carborane fragment through CH_2 spacers, along with their full characterization, are reported. Noticeable, bonding the *m*-carborane fragment to the anthracene moieties produces a significant increase of more than two-fold in the intrinsic fluorescence quantum yield (ϕ_F) of the anthracene itself, with values of ϕ_F > 60 % in THF and ϕ_F > 48 % in toluene, although do not alter the absorption and emission patterns of the fluorophore in solution. A red-shift of the emission maximum with respect to the solution is observed in the aggregate state (THF/H_2O, 1:99 v/v), along with moderate quantum yields; compounds **4** and **5** show ϕ_F = 22 and 19 %, respectively, whereas **6** has a lower value (ϕ_F = 8 %). The difference between the ϕ_F values in the aggregate state has been attributed to the arrangement of dimers for each compound in the solid state structures. X-ray crystal structures of compounds **4** and **5** show the anthracene units roughly parallel, whereas such arrangement is clearly disrupted in compound **6**. Such differences have been analyzed by Hirshfeld surfaces, decomposed fingerprint plots for the three compounds as well as DFT calculations. The combined results from the supramolecular analyses and DFT studies support the idea that a less delocalized system in the case of **6** can be explained by the different packing in the aggregate or solid state for this di-iodo derivative. The observed arrangement of molecules of **6** seems to be related to a larger number of H···I contacts, respect to the non-iodinated or mono-iodinated compounds, **4** or **5**. According to this assumption, there is a direct relationship between the structure in solid state and the PL properties; in the *m*-carborane derivatives, small changes in their structures have caused variations in the photophysical properties, especially in the quantum efficiency.

Introduction

Icosahedral carborane clusters, in particular dicarba-*closo*-dodecaboranes ($C_2B_{10}H_{12}$),[1-10] are highly chemical and thermally stable boron clusters,[11-13] characterized for their three-dimensional (3D) structure with electrons' delocalization inside the cage.[14, 15] These boron clusters possess a highly polarisable σ-aromatic character and interact electronically with π-conjugated systems.[16, 17] The *ortho*- (1,2-$C_2B_{10}H_{12}$) and *meta*-carborane (1,7-$C_2B_{10}H_{12}$) isomers have different electronic properties, as their electron-withdrawing capacity,[18] which has been found to be much larger for the *ortho* when compared to the *meta*-isomer.[19-21]. Owing to the intrinsic properties of carboranes, they have been used as exceptional building blocks for developing functional organic materials with enhanced thermal and chemical properties[22-25].

In the last decade, the development of boron cluster-based organic π-conjugated systems have attracted huge interest as active materials in (opto)electronic devices, such as organic light-emitting diodes (OLEDs), organic field effect transistors (OFETs), solar cells, biological sensors and imaging,[26-28] among others.[29, 30] It has been demonstrated the remarkable influence of the *o*-carborane cluster on the photophysical properties of luminescent materials in solution and solid state. Notably, when electron-donor or π-conjugated organic moieties are linked to the C atoms (C_c) of the *o*-carborane cage, it acts as an electron-withdrawing group. In that case, a photoinduced intramolecular charge transfer (ICT) process,[18] from the π-conjugated fragments to the antibonding orbital mostly placed on the C_c–C_c linkage,[31] takes place to produce a quenching of the fluorescence emission in solution.[21, 32-58] Nevertheless, these materials can recover the emission capacity in solid state thanks to the restriction of the intramolecular motion and C_c–C_c bond vibration. [59-64] Therefore, the *o*-carborane may be considered as a functional unit able to induce highly-efficient solid-state emissions in *o*-carborane conjugated materials in aggregation state. We have largely demonstrated over the years that using a non-conjugated spacer between the fluorophore and the C_c of the *o*-carborane

moiety typically prevents the ICT from the fluorophore to the electron-acceptor carborane in solution. But more interestingly, the fluorescence efficiency can be tailored by changing the substituent at the adjacent C_c position, which may cause either an enhancement of the emission quantum yield or a total fluorescence quenching in the case of aromatic substituents.[11-13, 65-69] Anthracene is a very well-studied π-conjugate system easy to functionalize and with remarkable intrinsic photophysical, photochemical and chemical properties, which make it and its derivatives ideal molecules to construct fluorophores, fluorescent probes, organic light-emitting transistors, among others.[70, 71] Throughout the last years, some carboranyl-functionalized anthracene derivatives have been reported and their photoluminescence behaviour explored.[35,68,72-75] In those systems in which the anthracene is directly linked to one or two *o*-carborane units through the C_c, or for these cases where there is a π-conjugated spacer between both fragments, a rapid ICT from the anthracene to the *o*-carborane occurs causing a quenching of the fluorescence in solution, whereas aggregation induced emission (AIE) in solid state or mechanochromic luminescence performance are observed.

Conversely, studies on *m*-carborane-based organic π-conjugated systems are scarce; for this reason the effect of the *m*-carborane fragment on the photophysical properties is less known as that for the *o*-carborane analogs.[11,35] It has been however observed that the binding of *m*-carborane to a fluorophore usually produces an important increase of the fluorescence compared to their *o*-carborane referents, both in solution and solid state.[11, 76] Noticeably, the *m*-carborane acts on one side, preventing the ICT due to the absence of the C_c-C_c bond and, on the other hand avoiding the strong π-π stacking. Then, the *m*-carborane can be converted into a very attractive scaffold for coupling a large variety of fluorophores.

Owing to our interest in elucidating the role of boron clusters in the luminescent properties of their derivatives, in the current work we have designed and synthesized novel fluorescent triads

in which the *m*-carborane is the bearer of anthracene units. Iodination of one and two B atoms is also performed to produce B-I vertices to study their possible influence in the photophysical behavior of the new fluorophores. Crystal structures of the synthesized compounds have been established by X-ray diffraction analysis. Experimental studies regarding photoluminescent properties in solution and aggregate state have been performed and complemented with theoretical calculations to establish meaningful structure-photophysical properties relationship for the compounds, in particular focused to elucidate the role of the *m*-carborane cluster. Regarding the solid state, it is known that well-defined molecules allow for crystalline materials, in which an adequate design of the molecular structure can lead to the specific intermolecular arrangements needed for optoelectronic properties.[77-79] One of the major challenges for the scientific community is to establish the structure–property relationships of a specific material, and understand how small changes in the molecular structure might impose large changes in solid state properties.

Results and discussion.

Synthesis and characterization of compounds 4–6. The synthesis of anthracenyl-disubstituted *m*-carborane derivatives **4–6** was easily achieved by nucleophilic substitution at the $C_{cluster}$ atoms (C_c) following a similar procedure to that previously used for the substitution of *o*- and *m*-carborane derivatives.[76,80] Compound **4** was obtained by nucleophilic substitution of 1,7-*closo*-$C_2B_{10}H_{12}$ (**1**), whereas **5** and **6** were obtained from the respective mono- and di-iodinated derivatives, 9-I-1,7-*closo*-$C_2B_{10}H_{11}$ (**2**) and 9,10-I_2-1,7-*closo*-$C_2B_{10}H_{10}$ (**3**), which were previously prepared by electrophilic substitution at the B atoms.[81] The reaction of the dilithium salts of **1–3** with two equiv. of 9-chloromethyl anthracene at reflux overnight yielded **4, 5** and **6**, respectively, in 68, 49 and 61% yield, respectively (Scheme 1). The nucleophilic

substitution reactions were monitored by $^{11}B\{^1H\}$ NMR following the appreciable changes in the boron resonances distributions.

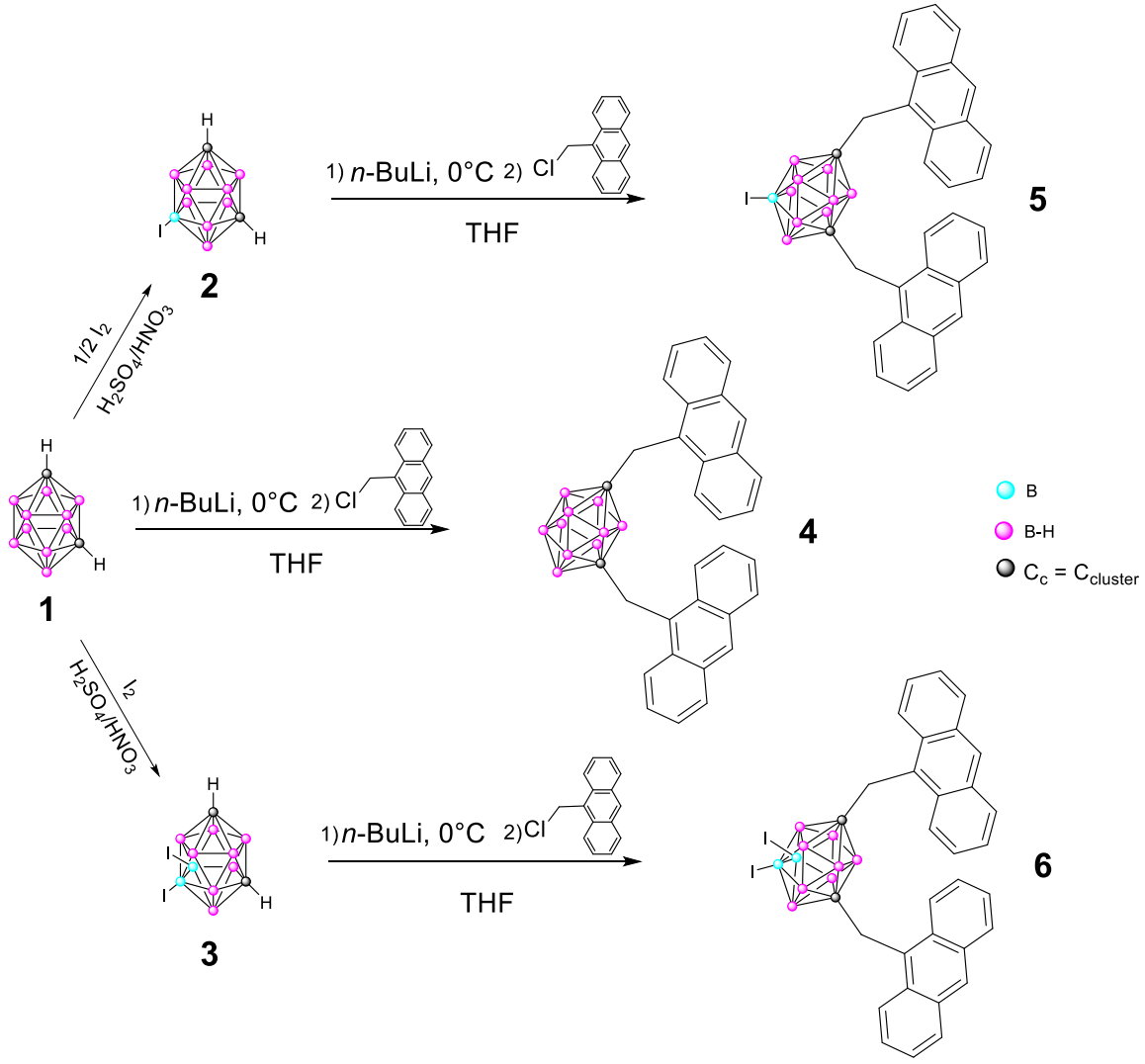

Scheme 1. Procedure leading to **4–6**.

The structures of **4–6** were established on the basis of IR, ^1H, $^{13}C\{^1H\}$ and $^{11}B\{^1H\}$ spectroscopy and elemental analysis; all of them were confirmed by X-ray diffraction analysis. The IR spectra of all compounds show typical υ(B-H) strong bands of *closo*-clusters between 2567 and 2632 cm^{-1}. ^1H NMR spectra of **4–6** display one singlet region, in the range from δ 4.11 to 4.08 ppm, attributed to the C_c-CH_2 protons. Due to the mono and diiodination of *m*-

carborane cluster, the $^{11}B\{^{1}H\}$ NMR spectra for the three compounds are different; non-iodinated *m*-carborane **4** and di-iodinated **6** show a more symmetric boron resonances distributions with a 2:6:2 and 2:4:2:2: patterns, respectively; on the other hand, the asymmetric mono-iodinated **5** shows a 2:5:1:1:1: pattern. As for previously reported iodinated derivatives,[76, 82, 83] the *B*-I are indubitably identified as the highest field resonances in the range from δ-21.15 to -23.87 ppm, which remain as a singlet in the $^{11}B\{^{1}H\}$ NMR. The $^{13}C\{^{1}H\}$ NMR spectra of **4–6** show the aromatic resonances in the range 131−124 ppm and a signal *C*H_2 carbon near δ = 33.60 ppm.

X-ray diffraction analysis of the crystal structures.

Single crystals suitable for X-ray structural determination of compounds **4**, **5** and **6** were obtained by slow evaporation from a mixture of chloroform/*n*-heptane (9:1) or dichloromethane at room temperature. The molecular structures for **4**, **5** and **6** were established by single crystal X-ray diffraction (Figure 1) and are in agreement with the NMR data (*vide supra*). Experimental crystal data and structure refinement parameters for the anthracenyl-containing carborane structures reported in this work are listed in Table 1. Whereas the *m*-carborane derivatives **4** and **6** both crystallize in the Monoclinic $P2_1/n$ space group, compound **5** crystallizes in the Orthorhombic $Pmc2_1$ space group. The molecular structures for all these compounds show typical icosahedron geometry with very similar bond distances and angles, and also similar to those in other disubstituted *m*-carboranyl compounds with aromatic rings connected through a methylene spacer.[84, 85]

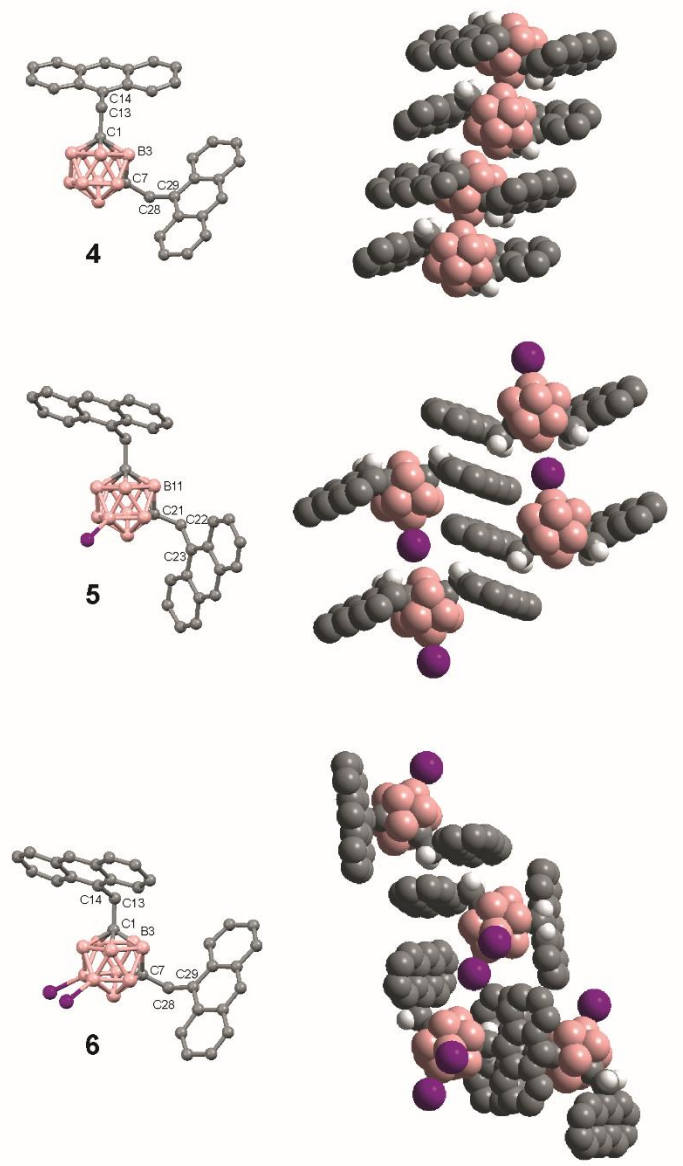

Figure 1. (Left column) Molecular structures of **4**, **5** and **6**. Torsion angles: **4** (C14C13C1B3, 33.7(2)°; C29C28C7B3, 107.6(2)°), **5** (C23C22C21B11, 173.9°), and **6** (C14C13C1B3, 29(1)°; C29C28C7B3, 108.1(8)°); (Right column) Projections showing the organization of four molecules of the compounds in the solid state. All H atoms, except those for the methylene –CH_2- groups, have been omitted for clarity. Color code: B pink; C grey; H white; I violet.

Table 1. Crystal data and refinement details for structures of compounds **4–6**.

	4	**5**	**6**
Empirical formula	$C_{32}H_{32}B_{10}$	$C_{32}H_{31}B_{10}I$	$C_{32}H_{30}B_{10}I_2$
Formula weight	524.67	650.57	776.46
Crystal system	Monoclinic	Orthorhombic	Monoclinic
Space group	$P2_1/n$	$Pmc2_1$	$P2_1/n$
Temperature/K	298	298	298
Wavelength/Å	1.54178	0.71073	0.71073
a/Å	14.9081(4)	18.808(3)	13.111(4)
b/Å	18.3536(6)	9.1786(13)	12.617(3)
c/Å	10.6137(4)	18.193(3)	19.401(5)
α/deg	90	90	90
β/deg	100.673(3)	90	92.596(9)
γ/deg	90	90	90
Volume/ $Å^3$	2853.85	3140.6(8)	3206.0(14)
Z	4	4	4
Density (calculated)/ Mg/m^3	1.221	1.376	1.609
F(000)	1096	1304	1512
Theta range for data collection/deg	3.016 to 66.748	2.166 to 27.505	2.241 to 25.027
Absorption coefficient/ mm^{-1}	0.464	1.042	1.985
Goodness-of-fit on F^2	1.055	1.044	1.040
R1[I>2sigma(I)]	0.0542	0.0291	0.0628
wR2[I>2sigma(I)]	0.1582	0.0690	0.1562
R1(all data)	0.0705	0.0417	0.0758
wR2(all data)	0.1702	0.0724	0.1655

CCDC 1853288 (**4**), 1853289 (**5**) and 1853290 (**6**) contain the supplementary crystallographic data for this paper. These data can be obtained free of charge from The Cambridge Crystallographic Data Centre via www.ccdc.cam.ac.uk/data_request/cif.

In all structures, the *m*-carborane moiety is linked to two anthracene units through a methylene spacer (-CH_2-). As shown in Figure 1, rotation of the anthracene rings through the (H)(H)C–C(anthracene) bond allows various conformations in the solid state. Conformations found in the solid state and torsion angles can be seen in Figure 1 caption. The dihedral angles between the two anthracene rings in **4–6** are 27.3°, 127.6/125.2° and 88.86°, respectively.

The solid state structures in **4–6** are mainly dominated by intermolecular C–H···π interactions (Figure 1 and Table 2). Notably, the presence of the -CH_2- spacer between the *m*-carborane and anthracene moieties seems to impede the *a priori* expected π···π interactions. Thus, extensive C–H···π interactions are found in all molecules, mainly between the -CH_2- hydrogen atoms and the aromatic anthracene rings (Figure 1 and Table 2). The distances of all of the observed intermolecular C–H···π contacts are in general substantially shorter than the 2.90 Å distance that corresponds to the sum of the van der Waals radii (∑vdW) of hydrogen and carbon atoms (Table 2) and the corresponding C–H···C(anthracene) angles are higher than 120º. Thus, they qualify as hydrogen bonds. Even though the packing in all compounds is essentially governed by C–H···π hydrogen bonds, the structures also show a high number of other weaker contacts as listed in Table 2. Those include C–H···H–B contacts in all structures and one B–H···I–B contact in **6**.

Table 2. Geometrical parameters of weak D–H···A (A = π, H, I, B) contacts (Å, º), involved in the supramolecular construction in **4–6**. For C–H···π contacts, geometries are given with respect to the aromatic centroid M or one of the ring carbons.

Compound	D–H···A	*d*(H···A)	<(DHA)	<(HHB)
4	C(24)–H(24)···C(17)^{i}	2.719	130.7	-
	C(28)–H(28A)···C(36)^{ii}	2.735	156.6	-
	C(13)–H(13A)···C(21)^{iii}	2.811	127.8	-
	C(32)–H(32)···H(9)–B(9)^{iv}	2.411	147.8	124.4
5	C(2)–H(2A)···M^{v}	2.792	130.1	-
	C(2)–H(2B)···M^{v}	2.854	128.8	-
	C(22)–H(22A)···M^{vi}	2.911	125.1	-
	C(22)–H(22B)···M^{vi}	2.775	133.4	-
	C(7)–H(7)···C(15)^{vii}	2.871	149.1	-
	C(34)–H(34)···C(7)^{viii}	2.866	152.9	-
	C(10)–H(10)···H(14A)–B(14)	2.264	155.1	145.2
	C(30)–H(30)···H(3)–B(3)	2.272	151.8	146.3
	C(35)–H(35)···H(12)–B(12)^{ix}	2.323	151.9	142.0
6	C(28)–H(28A)···M^{x}	2.846	138.8	-
	C(28)–H(28B)···M^{x}	2.713	126.3	-
	C(40)–H(40)···C(17)^{xi}	2.802	147.4	-
	C(40)–H(40)···C(18)^{xi}	2.817	132.8	-
	C(17)–H(17)···C(33)^{xii}	2.869	140.1	-
	C(38)–H(38)···H(6)–B(6)^{xiii}	2.417	144.3	167.9
	B(3)–H(3)···I(9)–B(9) ^{xiv}	3.187	129.8	-

Symmetry codes (i) 1-x,0.5+y,0.5-z (ii) x,0.5-y,-0.5+z (iii) x,0.5-y,0.5+z (iv) 2-x,-y,1-z (v) x,-1+y,z (vi) x,1+y,z (vii) x,1-y,-0.5+z (viii) x,1-y,0.5+z (ix) x,2-y,0.5+z (x) 1-x,1-y,1-z (xi) -0.5+x,0.5-y,0.5+z (xii) 1.5-x,-0.5+y,0.5-z (xiii) 0.5+x,0.5-y,0.5+z (xiv) 1.5-x,0.5+y,0.5-z.

Although the solid state structures in **4–6** are mainly dominated by intermolecular C–H···π interactions, the arrangement of molecules clearly differ (right column in Figure 1), which seems to be related with the presence of iodine atoms in the molecule. Whereas molecules of **4** and **5** arrange in a way that the anthracene rings are stacked in one direction and nearly parallel, this order is not observed in the solid state structure for **6** as molecules are organized in dimers that are twisted around 78º to one another.

Photophysical properties combined with TD-DFT calculations.

The photophysical properties of **4–6** were determined by UV-Vis absorption and fluorescence spectroscopy in solvents of different polarity (dioxane, THF and toluene), as well as in a mixture of THF/water (v/v = 1/99) to form aggregates (Table 3). Electronic properties of **4–6** in the ground state were assessed in different solvents by UV-Vis absorption measurements (~10^{-5} M, Figure 2). All compounds exhibit similar absorption spectra with a sharp band around 258 nm and four peaks at around 335, 351, 369 and 390 nm as show in Figures 2, with vibrational structures that were assigned to the π-π* transition band of the anthracene moiety; nevertheless none of them show an important solvatochromic effect. The molar absorption coefficients (ε) are somewhat different for the three compounds, and slight variations are observed for each compound in the different solvents; for compound **4** the **ε** values were in the range from 160×10^2 to 177×10^2 $M^{-1}cm^{-1}$, compound **5** exhibits the highest ε values of the three compounds within the range 185×10^2 to 207×10^2 $M^{-1}cm^{-1}$, whereas the diiodinated derivative **6** displays lower ε values than **4** and **5** (152×10^2-156×10^2 $M^{-1}cm^{-1}$). These results suggest that there is no correlation between the molar absorption coefficients and the number of iodine atoms in the molecule.

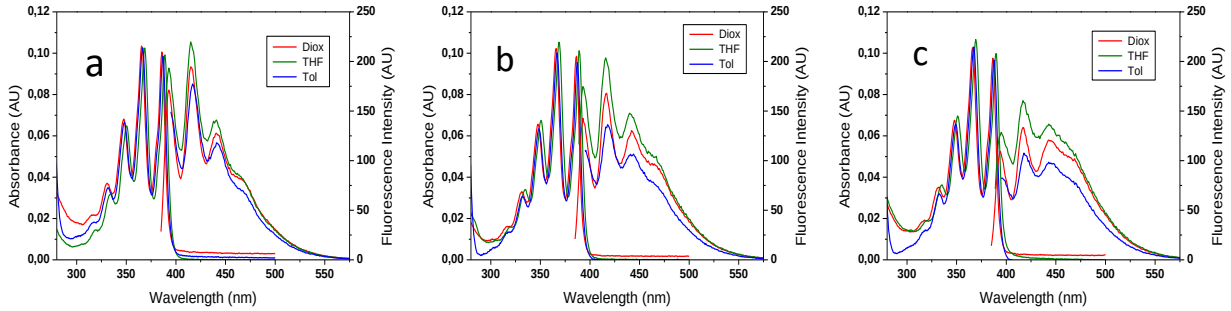

Figure 2. Absorption and emission spectra of **4** (a), **5** (b) and **6** (c) in THF (green), dioxane (red) and toluene (blue).

Photoluminescence (PL) emission spectra of **4–6** were also measured in various solvents, as well as in aggregate state (THF/H_2O = 1/99 (v/v). All of them show similar vibronic emission spectra in solution, with maxima around λ_{em} = 415–418 nm (Figure 2), that can be assigned to the local estate (LE) emission of the anthracene moiety, however no other bands at longer wavelengths (550–600 nm) due to intramolecular charge transfer (ICT) emission were observed, suggesting that no drastic conformational changes in the excited state occur. This is contrary to the previously reported anthracene-*o*-carborane dyads that exhibited dual emission around 450 and 600 nm with a quantum efficiency (ϕ_F) of 0.02, as the molecule had a parallel conformation that presented LE emission, whereas twisting occurred in the excited state, followed by the ICT emission.[73] The similarity between the spectra of **4–6** in solution to the anthracene itself (λ_{em} = 420 nm) suggested that only small electronic interactions between the anthracene units in the compounds takes place, independently of the substitution or not at the boron atoms of the carborane unit.

Remarkably, compounds **4–6** exhibit quantum yields (ϕ_F) in solution that are more than two-fold that for the single anthracene molecule (27% in EtOH or benzene).[86] Table 3 summarized the photophysical data for all the compounds. As it can be observed in Table 3, compounds **4–6** exhibit very similar fluorescence quantum yield values (ϕ_F) in each solvent (Table 3), being

significantly greater in the more polar solvent, THF (63–66 %), and lower in the less polar toluene (48–55%). The different fluorescence quantum yield (φ_F) values in the different solvents suggest that in polar solvents the radiative pathways are slightly dominant over non-radiative processes. However, this difference is not considered very relevant in this case. The high φ_F values indicate that there is no charge transfer in the molecule independent of the solvent polarity, which is in agreement with the frontier orbitals of the molecule (*vide infra*). It is worth noting that compounds **4–6** exhibit considerably higher fluorescence quantum yields in solution than their analogous bis-9-(methylene)anthracene-disubstituted *o*-carborane that contains two anthracene moieties linked to the C_c through a CH_2 moiety, which exhibited a ϕ_F = 9 %.[68] The decrease of fluorescence in the latter was then related with the C_c–C_c distance in the *o*-carborane, but obviously this is not the case for compounds **4–6,** which are derivatives of the *m*-carborane, therefore these results indicate that there are no CT contributions in the lowest excited state. This raises the question on how the *m*- isomer can influence to the intrinsic luminescence properties of the anthracene in solution; it is noticed that bonding the *m*-carborane to the anthracene moiety causes a geometrical effect instead of an electronic one, preventing intramolecular interactions that leads to an increase of more than two-fold in the quantum efficiency of anthracene itself. Besides, compounds **4–6** exhibit very similar fluorescence efficiency, despite the heavy-atom effect of iodine which is able to promote inter-system crossing (ISC); the apparently low ISC can be ascribed to the large distance between iodine and the anthracene units (*vide infra*).

Table 3. Photophysical data for compounds **4–6**.

Compounds	solvents	λ_{abs} (nm)	$\varepsilon/10^5$ (M^{-1} cm^{-1})	λ_{em}(nm)	ϕ_F[a]	Stokes shift (nm)
4	Dioxane	365	0.177	415	0.59	50
	Toluene	367	0.177	417	0.55	50
	THF	369	0.160	415	0.63	46
	THF/water (1:99)	373	–	461	0.22	88
5	Dioxane	366	0.200	417	0.60	51
	Toluene	367	0.207	418	0.53	51
	THF	369	0.185	416	0.66	47
	THF/water (1:99)	374	–	460	0.19	86
6	Dioxane	366	0.156	417	0.57	51
	Toluene	367	0.152	418	0.48	51
	THF	369	0.156	417	0.63	48
	THF/water (1:99)	375	–	464	0.08	89

[a] Reference compound Quinine sulfate (0.5 M H_2SO_4, ϕ_F = 0.54)

To better understand the photophysical properties of the investigated systems, we carried out DFT (B3LYP) calculations (see S.I. for details). In previous studies in our group[87] and in others[88], it was clearly demonstrated that the 6-31G* basis set (although a rather small basis set) describes well the photophysical properties of these carborane containing systems. Different rotamers of **4**, **5** and **6** (including those found in the crystal structures of **4(cryst), 5(cryst)** and **6(cryst**)) were optimized; their relative energies were compared at B3LYP/6-31G* level of theory and further single point calculations were performed at B3LYP/6-311+G** (for the iodine atom LANL2DZ) level of theory (Figures S1-S3 in S.I.). As mentioned above, the results are certainly comparable and therefore the smaller basis set describes well the photophysical properties of **4–6**. The energy differences between the rotamers are very small (<1.2 kcal/mol), which indicate that there is no preferred orientation of the substituents in the gas phase.

According to the Kohn-Sahm frontier molecular orbitals, two types of rotamers can be distinguished (Figure 3 and Figures S4-S7 in SI). In the first type of the rotamers (Type I), both anthracene units have contribution to the frontier orbitals (e.g. **4(cryst)** and **5(cryst)**

in Figure 3), while in the case of the second type of rotamers (Type II) the frontier orbitals are localized only at one of the anthracenyl-groups (e.g. **6(cryst)** in Figure 3). There are no trends in the stability of the type of rotamers and also the energy difference between the frontier orbitals are the same ($\Delta\varepsilon$<0.3 eV), and the energy differences between the rotamers is small, so that most probably there is no preferred orientation in solution.

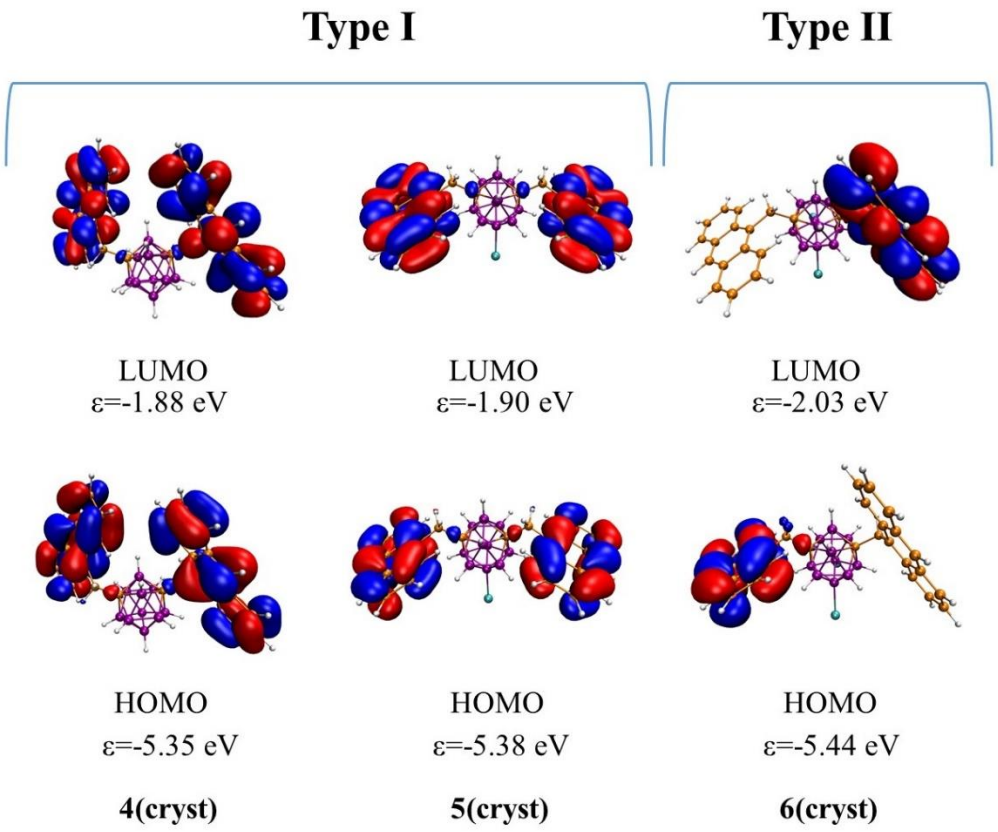

Figure 3. Kohn-Sahm orbital of monomers of **4(cryst)**, **5(cryst)** and **6(cryst)**. The geometry optimizations were started from the crystal structures.

The TD-DFT calculations (Table S1-S18 in SI) verify the local excitation mode of the transitions in the case of the first type of rotamers (Type I in Figure 3) in the region of 370-400 nm, however, in the case of the second type (Type II in Figure 3) there are transitions in which the transfer occurs between two different anthracene units, indicating that the system has some charge transfer character (Table S19). Further rotamers and their frontier

orbitals are represented in Figure S3-S7 of the SI. As expected, the absorption peaks of the calculated transitions for the Type II rotamers are redshifted (370-420 nm), however, their oscillator strength (f) is significantly lower when compared with the similar transitions for the Type I rotamers (e.g the first excited states of **4(cryst)**, **5(cryst)** and **6(cryst)** in Tables S1, S7 and S13, respectively). Since the calculated oscillator strength (which corresponds to the intensity of the peaks in the experimental spectra) of these transitions in the Type II rotamers are significantly smaller, the redshifted character was not observed experimentally. As the figures in Table S19 show, the first 4 lowest transitions of **4(cryst)** and **5(cryst)** exhibit local transition mode, so that there is no charge transfer between the different parts of the molecules. In the case of **6(cryst)** the first and the fourth lowest transitions have CT character; the charge transfer occurs between the two anthracene units, but as it was stated above the oscillator strength of these transitions are significantly lower (f = 0.001) than the local excitations in case of Type I rotamers of **6** (compare the f values in Table S13-S18). It should be noted that all of the calculated results were in good agreement with the experimentally observed spectra, in which we have not observed red-shifted absorption. The above calculated and experimental results provides evidence that there are no intense CT transition in the lowest excited states. Owing to the fact that the lone pairs of the iodine atoms are in the border orbitals' region (e.g: HOMO-2, HOMO-3 in case of **5** and **6,** Figure S4 in SI), they are not involved in these transitions. Besides the large distance between the iodo and the anthracene substituents, the reason why the iodo substituents do not affect the emission/absorption is the lower energy level of the lone pairs of these iodo substituents in **5** and **6**.,which have lower energy by ~1 eV than the π system of the anthracene (Figure S4), thus it cannot so easily interact with other orbitals. Finally, we investigated the PL behavior in aggregate state (THF/H_2O = 1/99 (v/v)); emission spectra of **4–6** are shown in Figure 4. The PL spectra for these compounds are very similar, showing non-

vibronic structures and a maximum emission around 463 nm (Table 3), red-shifted respect to the THF solutions. Consequently, larger Stokes shifts are also observed. Noticeable, higher fluorescence quantum yields were determined for **4** (ϕ_F = 22 %) and **5** (ϕ_F = 19 %) with respect to diiodinated **6**, in which the quantum yield drops to 8 %; although these values represent a decrease when compared to the respective ones in solution, there is a significant difference between the ϕ_F values between **4**-**5** and **6** aggregates (Table 3) that are worth studying.

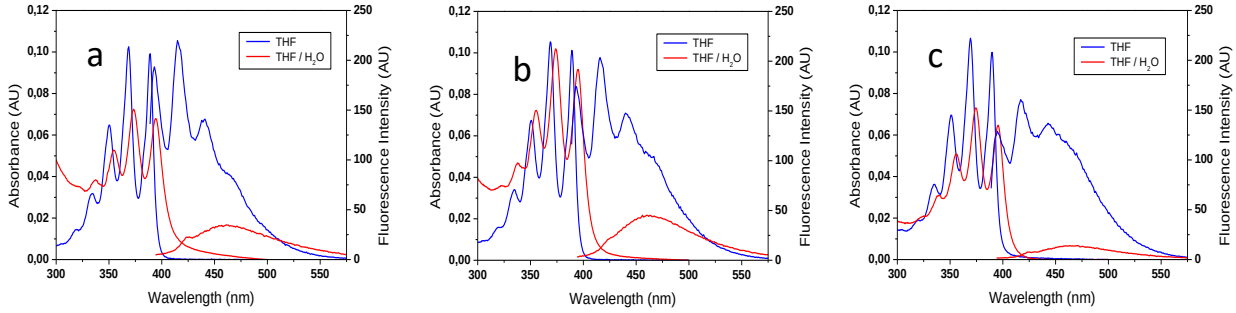

Figure 4. Absorption and emission spectra of **4** (a), **5** (b) and **6** (c) in THF solution (~10^{-5} M) and aggregates (THF/H_2O, v/v = 1/99, 10^{-5} M).

The photophysical properties in the aggregate state are complicated and difficult to control as those are not only related to the electronic properties of the molecules but also to their supramolecular structures in the aggregate or solid state. Thus, understanding the nature of the intermolecular interactions that determine the aggregation of molecules in saturated solutions or packing of molecules in the solid state, and how they may affect the optical and electronic properties of the materials is certainly essential for tuning their properties.[89] Aggregates of **4–6** in THF/water (1:99) can in principle be, either metastable amorphous or stable crystalline phases.[90] Solid powders of **4–6**, obtained by fast precipitation during their syntheses, show powder X-ray diffraction (PXRD) patterns that match the calculated patterns from the X-ray structures of the compounds (Figure S9-11). This is remarkable as pure phases are obtained in

all cases under non thermodynamic conditions (e.g., slow crystallization) and no polymorphism is observed. Therefore, these data suggest that the aggregates of **4–6** in THF/water (1:99) should be likely stable crystalline phases. Nevertheless, and in order to try to understand the difference between the fluorescent quantum yields of aggregates of **4**-**5** and **6**, we have further analyzed the supramolecular structures for these molecules in their solid structures (Figure 1). Thus, we have analyzed the Hirshfeld surfaces and decomposed fingerprint plots for the three compounds (see full data and details in the SI).[91] This is a very valuable method for the analysis of intermolecular contacts that offer a whole-of-the-molecule approach.[92] This method enables separation of contributions from different interaction types to the solid state structures and facilitates the rapid comparison between related molecules in the same or different crystals.[93] Figure 5 represents the fraction of the Hirshfeld surface representing a given interaction for each compound (see SI for details). From this simple analysis, it immediately emerges that H···H contacts comprise nearly 70% of the total Hirshfeld surface area for the non-iodinated compound **4** and 56% or 47% for the iodinated, **5** or **6**, respectively. This is not surprising taking into account the large ratio of external H to C or I atoms in each molecule due to the carborane cages and anthracene rings. H···C contacts (e.g., C–H···π) contribute around 25-29% to the total Hirshfeld surface area for the three compounds. The contribution of H···I interactions varies from 14% to 20% from **5** to **6**, respectively. Finally, a small percentage of C···C contacts (e.g., π···π interactions) are found in all compounds and additional small percentage of C···I contacts in **6**. As clearly seen in Figure 5, the major difference between **6** and **4**-**5** is a significantly larger percentage of H···I interactions in the first one.

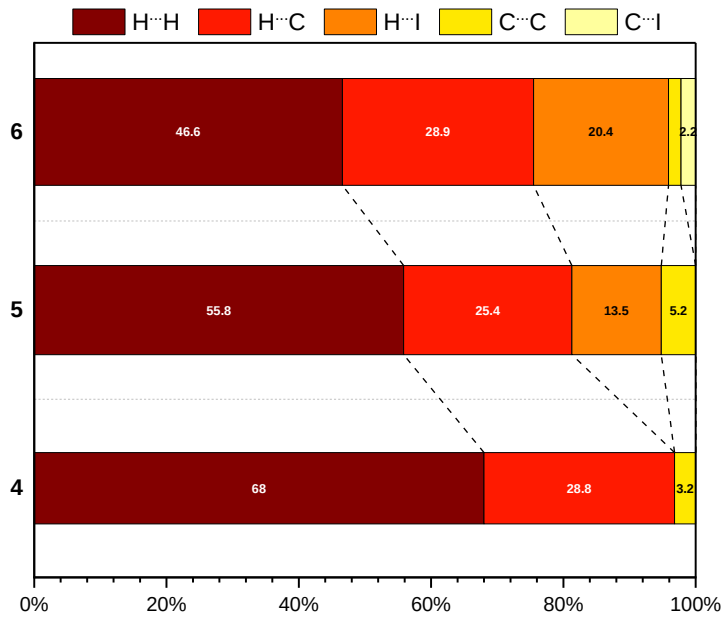

Figure 5. Relative contributions of various intermolecular contacts to the Hirshfeld surface area in all compounds in this study.

As we mentioned earlier, the arrangement of the anthracenyl moieties in the solid state of **6**, clearly differ from those for **4** and **5** (Figure 1). The different arrangement of dimers in **6** might be due to a combination of the molecular structure (e.g., different rotamers) and its supramolecular chemistry (e.g., H···I interactions). In any case, such different arrangement in **6** might explain its higher quantum yield drop in the aggregate state. In order to verify this hypothesis, we have selected the tetrameric structures for **4–6**, shown in Figure 1 (these repeating units represents well the crystal structure) and their Kohn-Sahm orbitals were calculated (Figure 6).

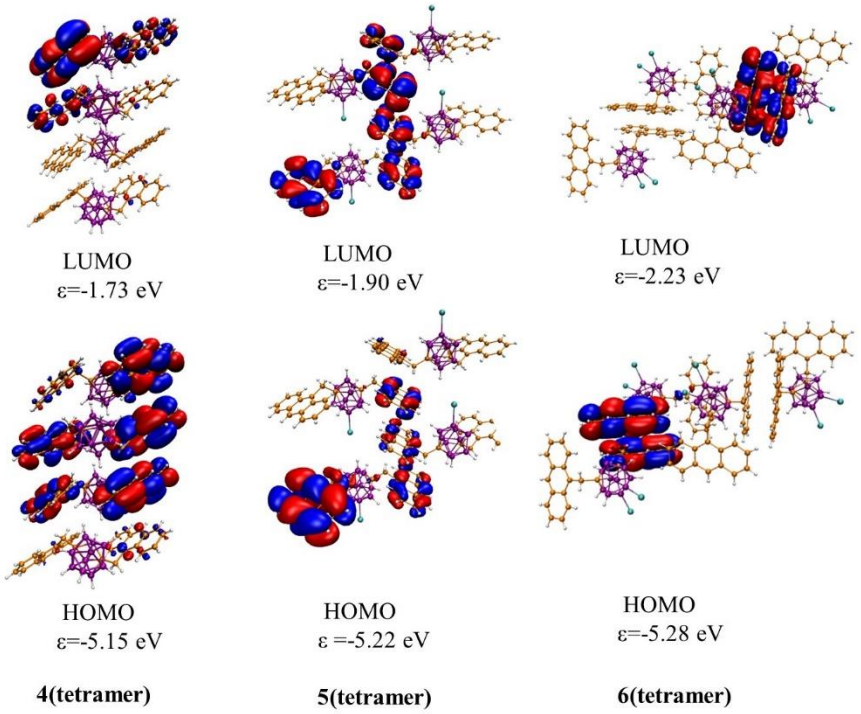

Figure 6. Kohn-Sahm frontier orbitals of the tetrameric structures of **4–6**. The geometries were taken from the X-ray structures and used without further optimization.

The results presented in Figure 6 clearly show a significant delocalization on the frontier orbitals of the tetramers in **4(tetramer)** and **5(tetramer)**, together with a decrease of the energy difference between the orbitals (both occupied and unoccupied) respect to those in the monomers (Figure S4). Further orbitals from the frontier orbital region are given in Figure S8 of the S.I. Interestingly, the unoccupied orbitals of **6(tetramer)** (LUMO+X, X=0-3) are delocalized mainly only in one of the dimeric unit, while in the case of **4(tetramer)** and **5(tetramer)** the unoccupied orbitals spread over more significantly. The larger delocalization was also indicated by the energy difference between these orbitals; while the energy difference between the LUMO and LUMO+3 in case of the **4(tetramer)** and **5(tetramer)** is only 0.06 eV and 0.08 eV, in case of **6(tetramer)** it is considerably higher (0.31 eV). The reason of the higher

delocalization in case of **4**(**tetramer)** and **5**(**tetramer)** can be attributed to the stacked and nearly parallel anthracene units, while in case of **6**(**tetramer)** they are rather twisted, which prevents the further delocalization. This difference could be the reason of the lower quantum yield in aggregate state in case of **6** comparing with **4** and **5**, since the higher density of electronic states in case of **4** and **5** and the significant delocalization of the unoccupied orbitals between the molecules allow relaxation from higher-lying excited states via lower excited states (internal conversion), thus the emission will dominate instead of the non-radiative processes.[94] Thus, the DFT calculations support the idea that the different packing in the crystal structure of **6** causes the lower quantum yield. In contrast to the supramolecular structures of **4** and **5** (Figure 1), in which each anthracene unit has two neighboring anthracenes from other molecules which are roughly parallel, dimers of **6** are packed twisted. The later seems to avoid or diminish the interaction between the π-systems which could have an impact in the photophysical properties.

Conclusions

The *m*-carborane has demonstrated to be a perfect platform to boost the photoluminescent properties of fluorophores linked to it. An increase of more than two-fold in the intrinsic fluorescence efficiency of the anthracene itself (27% in EtOH) is produced when this fluorophore is bound through C_c–CH_2 to the non- (**4**), mono- (**5**) or di-iodinated (**6**) *m*-carborane fragments, giving rise to high fluorescence quantum yields in solution (>60% in THF). Remarkably, we have demonstrated that, contrary to previous findings for *o*-carborane triads, the above *m*-carborane compounds are good emitters in solution, while retaining also fluorescence emission in the aggregate state. While the non-iodinated and mono-iodinated compounds (**4** and **5**) show moderate quantum yields (ϕ_F = 22 and 19%), the di-iodinated compound **6** drops to a ϕ_F = 8%. The differences in the quantum efficiency in the aggregate

state seems to be related to the arrangement of dimers for each compound in the solid state structures. Analysis by Hirshfeld surfaces and decomposed fingerprint plots for the three compounds and DFT calculations are supportive of this assumption. The combined results from the supramolecular analyses and DFT support the idea that a less delocalized system in the case of **6**, due to a larger number of H···I contacts, can explain the different packing in the aggregate or solid state. All these results clearly indicate that small modifications in the molecular structure can lead to significant variations of the PL properties, especially in the quantum efficiency. This evidences that in the *m*-carborane derivatives the photophysical properties can be properly modified by the type of functionality and number of substituents. In our systems, the iodinated (B-I) species can be modified by introducing other functions by B-coupling reactions. Work in this direction is underway.

Experimental

Instrumentation. Elemental analyses were performed using a Carlo Erba EA1108 microanalyzer. ATR-IR spectra were recorded on JASCO FT/IR-4700 spectrometer on a high-resolution. The ^{1}H NMR (300.13 MHz), ^{11}B {^{1}H} (96.29 MHz) and ^{13}C {^{1}H} NMR (75.47 MHz) spectra were recorded on a Bruker ARX 300 spectrometer. All NMR spectra were recorded in $CDCl_3$ solutions at 25 ºC. Chemical shift values for ^{11}B {^{1}H} NMR spectra were referenced to external $BF_3{\cdot}OEt_2$, and those for ^{1}H and ^{13}C {^{1}H} NMR were referenced to $SiMe_4$ (TMS). Chemical shifts are reported in units of parts per million downfield from the reference, and all coupling constants are reported in Hertz. UV-Vis spectra were recorded on VARIANT Cary 5 UV-Vis-NIR spectrophotometer, using spectroscopic grade dioxane, THF and toluene (Sigma-Aldrich), in normal quartz cuvette having 1 cm path length, for different solutions for each compound in the range 5×10^{-5} to 1×10^{-5} M in order to calculate the molar extinction coefficients (ε). The fluorescence emission spectra and excitation spectra for all samples were

recorded in a VARIANT Cary Eclipse Fluorescence spectrometer. No fluorescent contaminants were detected on excitation in the wavelength region of experimental interest. The fluorescence quantum yields were determined by the "single point method" and repeated three times with similar optical density for reproducibility, against quinine sulfate in 0.5 M aqueous sulfuric acid with $\phi_F = 0.54$ as a standard.[95] For the suspensions in THF/water (1/99, v/v) the refractive index was assumed to be that of pure water (1.33). Powder X-ray Diffraction (PXRD) patterns were recorded at room temperature on an X'Pert PRO MPD diffractometer (Panalytical) using Cu Kα (λ = 1.5405 Å) radiation.

Materials. All reactions were performed under atmosphere of dinitrogen employing standard Schlenk techniques. Tetrahydrofuran was purchased from Merck and distilled from sodium benzophenone prior to use. Commercial grade diethyl ether, hexane, petroleum ether, *n*-heptane, chloroform and dichloromethane were used without further purification. 1,7-*closo*-$C_2B_{10}H_{12}$ (**1**) was supplied from KatChem Ltd. (Prague) and used as received. Compounds 9-I-1,7-dicarba-*closo*-dodecaborane (**2**) and 9,10-I_2-1,7-dicarba-*closo*-dodecaborane (**3**) were synthesized according to the literature. *n*-BuLi solution (1.6 M in hexane) was purchased from Aldrich and 9-(chloromethyl)anthracene was purchased from Alfa Aesar.

X-ray single-crystal structure determination.

Measured crystals were prepared under inert conditions immersed in perfluoropolyether as protecting oil for manipulation. Suitable crystals were mounted on MiTeGen Micromounts™ and these samples were used for data collection. Data were collected with a Bruker D8 Venture diffractometer. The data were processed with APEX3 suite.[A.S. Bruker, Bruker AXS Inc. V2016.1, 2016, Madison, Wisconsin, USA] The structures were solved by direct methods,[96] which revealed the position of all non-hydrogen atoms. These atoms were refined on F^2 by a

full-matrix least-squares procedure using anisotropic displacement parameters. All hydrogen atoms were located in difference Fourier maps and included as fixed contributions riding on attached atoms with isotropic thermal displacement parameters 1.2 times those of the respective atom. Crystallographic data for the structure of compounds **4**, **5** and **6** have been deposited with the Cambridge Crystallographic Data Center as supplementary publication no. CCDC 1853288-1853290. Geometric calculations and molecular graphics were performed with Mercury.[97] Additional crystal data are shown in Tables 1 and S1. Copies of the data can be obtained free of charge at http://www.ccdc.cam.ac.uk/products/csd/request/.

Synthesis of 4. A dry 25 mL round-bottomed flask equipped with a magnetic stirring bar was charged under nitrogen with a solution of **1** (0.300 g, 2.08 mmol) in THF (10 mL) at 0°C. Then, a solution of *n*-BuLi 1.6 M in hexanes (2.73 mL, 4.37 mmol) was added dropwise to the mixture, which was allowed to stir for 1 h at room temperature and cooled again at 0°C. A solution of 9-chloromethyl anthracene (0.993 g, 4.29 mmol) in THF (7.5 mL) was then added dropwise to the mixture under vigorous stirring. Then it was stirred for half hour at room temperature and heated to reflux overnight. After that, the solvent was removed under vacuum and the residue was quenched with H_2O (10 mL), transferred to a separating funnel, and extracted with Et_2O (3 × 10 mL). The organic layer was dried over $MgSO_4$ and the volatiles were reduced under vacuum. The orange oil residue was purified by silica gel column chromatography (dichloromethane/hexane 1:9) to give **4** as a yellowish white solid. Yield: 0.742 g, 68%. Crystals suitable for X-ray analysis were obtained by slow evaporation from a solution of **4** in a mixture of chloroform/*n*-heptane (9:1). ^{1}H NMR, δ (ppm) = 8.40 (s, 2H, $C_{14}H_9$), 7.97 (d, ^3J (H,H) = 9 Hz, 4H, $C_{14}H_9$), 7.93 (d, ^3J (H,H) = 9 Hz, 4H, $C_{14}H_9$), 7.44 (t, ^3J (H,H) = 7.5 Hz, 4H, $C_{14}H_9$), 7.36 (t, ^3J (H,H) = 7.5 Hz, 4H, $C_{14}H_9$), 4.11 (s, 4H, CH_2); ^{11}B{^{1}H} NMR, δ(ppm) = –6.19 (s, 2B), –11.03 (s, 6B), –13.27 (s, 2B); ^{13}C{^{1}H} NMR, δ (ppm) = 131.39

(s, $C_{14}H_9$), 130.75 (s, $C_{14}H_9$), 129.40 (s, $C_{14}H_9$), 129.19 (s, $C_{14}H_9$), 128.17 (s, $C_{14}H_9$), 126.23 (s, $C_{14}H_9$), 125.00 (s, $C_{14}H_9$), 124.68 (s, $C_{14}H_9$), 75.97 (s, C_c), 33.77 (s, CH_2); ATR-IR (cm^{-1}): ν = 3086, 3050, 2954, 2919, 2850 (C_{ar}–H), 2625, 2615, 2567 (B–H), 1624 (C=C); elemental analysis calcd. (%) for $C_{32}H_{32}B_{10}$: C, 73.25; H, 6.15. Found: C, 73.67; H, 6.94.

Synthesis of 5. The procedure was the same as for **4**, but using a solution of **2** (0.300 g, 1.11 mmol) in THF (5 mL), *n*-BuLi 1.6 M in hexanes (1.46 mL, 2.34 mmol) and a solution of 9-chloromethyl anthracene (0.540 g, 2.33 mmol) in THF (4 mL). After extraction with 3 × 10 mL of brine/CH_2Cl_2 the orange oil was purified by silica gel column chromatography (dichloromethane/petroleum ether 2:8) to give **5** as a yellow solid. Yield: 0.353 g, 49%. Crystals suitable for X-ray analysis were obtained by slow evaporation from a solution of **5** in a mixture chloroform/*n*-heptane (9:1). ^{1}H NMR, δ (ppm) = 8.39 (s, 2H, $C_{14}H_9$), 7.96 (d, ^3J (H,H) = 9 Hz, 4H, $C_{14}H_9$), 7.85 (d, ^3J (H,H) = 9 Hz, 4H, $C_{14}H_9$), 7.43 (t, ^3J (H,H) = 7.5 Hz, 4H, $C_{14}H_9$), 7.36 (t, ^3J (H,H) = 9 Hz, 4H, $C_{14}H_9$), 4.08 (s, 4H, CH_2); ^{11}B{^{1}H} NMR, δ(ppm) = –5.26 (s, 2B), –9.70 (s, 5B), –13.22 (s, 1B), –15.43 (s, 1B), –23.87 (s, 1B); ^{13}C{^{1}H} NMR, δ (ppm) = 131.36 (s, $C_{14}H_9$), 130.64 (s, $C_{14}H_9$), 129.28 (s, $C_{14}H_9$), 128.67 (s, $C_{14}H_9$), 128.44 (s, $C_{14}H_9$), 126.44 (s, $C_{14}H_9$), 125.06 (s, $C_{14}H_9$), 124.30 (s, $C_{14}H_9$), 33.61 (s, CH_2); ATR-IR (cm^{-1}): ν = 3081, 3055 (C_{ar}–H), 2613, 2590 (B–H), 1623 (C=C); elemental analysis calcd. (%) for $C_{32}H_{31}B_{10}I$: C, 59.07; H, 4.80. Found: C, 59.46; H, 4.86.

Synthesis of 6. The procedure was the same as for **4**, but using a solution of **3** (0.300 g, 0.758 mmol) in THF (5 mL), *n*-BuLi 1.6 M in hexanes (1.00 mL, 1.60 mmol) and a solution of 9-chloromethyl anthracene (0.368 g, 1.59 mmol) in THF (4 mL). After extraction with 3 × 10 mL of brine/CH_2Cl_2 the orange oil was purified by silica gel column chromatography (dichloromethane/petroleum ether 2:8) to give **6** as a yellow solid. Yield: 0.359 g, 61%. Crystals

suitable for X-ray analysis were obtained by slow evaporation from a solution of **6** in dichloromethane. ^{1}H NMR, δ (ppm) = 8.41 (s, 2H, $C_{14}H_9$), 7.97 (d, ^{3}J (H,H) = 9 Hz, 4H, $C_{14}H_9$), 7.80 (d, ^{3}J (H,H) = 9 Hz, 4H, $C_{14}H_9$), 7.44 (t, ^{3}J (H,H) = 7.5 Hz, 4H, $C_{14}H_9$), 7.35 (t, ^{3}J (H,H) = 7.5 Hz, 4H, $C_{14}H_9$), 4.10 (s, 4H, CH_2); ^{11}B{^{1}H} NMR, δ(ppm) = –4.01 (s, 2B), –9.58 (s, 4B), –15.22 (s, 2B), –21.15 (s, 2B); ^{13}C{^{1}H} NMR, δ (ppm) = 131.34 (s, $C_{14}H_9$), 130.57 (s, $C_{14}H_9$), 129.38 (s, $C_{14}H_9$), 128.71 (s, $C_{14}H_9$), 128.07 (s, $C_{14}H_9$), 126.69 (s, $C_{14}H_9$), 125.16 (s, $C_{14}H_9$), 123.99 (s, $C_{14}H_9$), 33.55 (s, CH_2); ATR-IR (cm^{-1}): ν = 3083, 3050 (C_{ar}–H), 2632, 2616, 2604, 2580 (B–H), 1624 (C=C); elemental analysis calcd. (%) for $C_{32}H_{30}B_{10}I_2$: C, 49.50; H, 3.89. Found: C, 49.90; H, 3.98.

Electronic Supplementary Information: Electronic supplementary Information for this article include ^{1}H and ^{11}B{^{1}H} NMR spectra, computational details, crystallographic data, powder diffraction data and Hirshfeld Surface Analyses for all the compounds. The data are available free of charge via the Internet at http://doi.org/

Conflict of interest

The authors declare no conflict of interest.

Acknowledgments. The work was supported by Spanish Ministerio de Economía y Competitividad, MINEICO (CTQ2016-75150-R and "Severo Ochoa" Program for Centers of Excellence in R&D SEV- 2015-0496) and Generalitat de Catalunya (2017/SGR/1720). ZK is grateful for the general support of the European Union's Horizon 2020 research and innovation program under the Marie Skłodowska-Curie grant agreement MSCA-IF-2016-751587. Theoretical calculations have been achieved using computers from Supercomputing Centre of Catalonia (CESCA).

References

1. J. Zhang and Z. Xie, *Acc. Chem. Res.*, 2014, **47**, 1623-1633.
2. N. S. Hosmane, *Boron Science: New Technologies and Applications*, Taylor & Francis, 2011.
3. Z.-J. Yao and G.-X. Jin, *Coord. Chem. Rev.*, 2013, **257**, 2522-2535.
4. M. Scholz and E. Hey-Hawkins, *Chem. Rev.*, 2011, **111**, 7035-7062.
5. F. Issa, M. Kassiou and L. M. Rendina, *Chem. Rev.*, 2011, **111**, 5701-5722.
6. V. I. Bregadze, *Chem. Rev.*, 1992, **92**, 209-223.
7. A. M. Spokoyny, *Pure Appl. Chem.*, 2013, **85**, 903-919.
8. F. Teixidor, C. Viñas, A. Demonceau and R. Nuñez, *Pure Appl. Chem.*, 2003, **75**, 1305-1313.
9. R. N. Grimes, *Carboranes*, Academic Press, US, 2016.
10. C. V. F. Teixidor, in *Science of Synthesis*, Thieme Stuttgart, 2005, vol. 6, pp. 1235-1275.
11. J. Cabrera-González, A. Ferrer-Ugalde, S. Bhattacharyya, M. Chaari, F. Teixidor, J. Gierschner and R. Núñez, *J. Mater. Chem. C*, 2017, **5**, 10211-10219.
12. A. Ferrer-Ugalde, E. J. Juárez-Pérez, F. Teixidor, C. Viñas and R. Núñez, *Chem. Eur. J.*, 2013, **19**, 17021-17030.
13. A. González-Campo, A. Ferrer-Ugalde, C. Viñas, F. Teixidor, R. Sillanpää, J. Rodríguez-Romero, R. Santillan, N. Farfán and R. Núñez, *Chem. Eur. J.*, 2013, **19**, 6299-6312.
14. P. Jordi, S. Miquel, V. Clara and T. Francesc, *Chem. Eur. J.*, 2013, **19**, 4372-4372.
15. P. Jordi, S. Miquel, V. Clara and T. Francesc, *Angew. Chem. Int. Ed.*, 2014, **53**, 12191-12195.
16. R. Kivekäs, R. Sillanpää, F. Teixidor, C. Viñas and R. Núñez, *Acta Cryst. C-Cryst. Struct. Commun.*, 1994, **50**, 2027-2030.
17. R. Sillanpää, R. Kivekäs, F. Teixidor, C. Viñas and R. Núñez, *Acta Cryst. C-Cryst. Struct. Commun.*, 1996, **52**, 2223-2225.
18. R. Núñez, P. Farràs, F. Teixidor, C. Viñas, R. Sillanpää and R. Kivekäs, *Angew. Chem. Int. Ed.*, 2006, **45**, 1270-1272.
19. N. Tsuboya, M. Lamrani, R. Hamasaki, M. Ito, M. Mitsuishi, T. Miyashita and Y. Yamamoto, *J. Mater. Chem.*, 2002, **12**, 2701-2705.
20. O. Crespo, M. C. Gimeno, A. Laguna, I. Ospino, G. Aullon and J. M. Oliva, *Dalton Trans.*, 2009, 3807-3813.
21. L. Weber, J. Kahlert, R. Brockhinke, L. Böhling, A. Brockhinke, H.-G. Stammler, B. Neumann, R. A. Harder and M. A. Fox, *Chem. Eur. J.*, 2012, **18**, 8347-8357.
22. A. L. Chan, J. Estrada, C. E. Kefalidis and V. Lavallo, *Organometallics*, 2016, **35**, 3257-3260.
23. R. M. Dziedzic, L. M. A. Saleh, J. C. Axtell, J. L. Martin, S. L. Stevens, A. T. Royappa, A. L. Rheingold and A. M. Spokoyny, *J. Am. Chem. Soc.*, 2016, **138**, 9081-9084.
24. B. J. Eleazer, M. D. Smith, A. A. Popov and D. V. Peryshkov, *J. Am. Chem. Soc.*, 2016, **138**, 10531-10538.
25. S. P. Fisher, A. El-Hellani, F. S. Tham and V. Lavallo, *Dalton Trans.*, 2016, **45**, 9762-9765.
26. M. Chaari, N. Gaztelumendi, J. Cabrera-González, P. Peixoto-Moledo, C. Viñas, E. Xochitiotzi-Flores, N. Farfán, A. Ben Salah, C. Nogués and R. Núñez, *Bioconjugate Chem.*, 2018, **29**, 1763-1773.
27. B. M. Muñoz-Flores, J. Cabrera-González, C. Viñas, A. Chavez-Reyes, H. V. R. Dias, V. M. Jiménez-Pérez and R. Núñez, *Chem. Eur. J.*, 2018, **24**, 5601-5612.
28. C. Bellomo, M. Chaari, J. Cabrera-González, M. Blangetti, A. Deagostino, C. Lombardi, C. Viñas, N. Gaztelumendi, C. Nogués, R. Núñez and C. Prandi, *Chem. Eur. J.*, 2018, **DOI: 10.1002/chem.201802901**.
29. R. Núñez, M. Tarrés, A. Ferrer-Ugalde, F. F. de Biani and F. Teixidor, *Chem. Rev.*, 2016, **116**, 14307-14378.
30. S. Mukherjee and P. Thilagar, *Chem. Commun.*, 2016, **52**, 1070-1093.
31. J. Llop, C. Viñas, F. Teixidor, L. Victori, R. Kivekäs and R. Sillanpää, *Organometallics*, 2001, **20**, 4024-4030.

32. H. Naito, K. Nishino, Y. Morisaki, K. Tanaka and Y. Chujo, *J. Mater. Chem. C*, 2017, **5**, 10047-10054.
33. Y.-J. Cho, S.-Y. Kim, M. Cho, W.-S. Han, H.-J. Son, D. W. Cho and S. O. Kang, *Phys. Chem. Chem. Phys.*, 2016, **18**, 9702-9708.
34. Z. Wang, P. Jiang, T. Wang, G. J. Moxey, M. P. Cifuentes, C. Zhang and M. G. Humphrey, *Phys. Chem. Chem. Phys.*, 2016, **18**, 15719-15726.
35. D. Tu, P. Leong, Z. Li, R. Hu, C. Shi, K. Y. Zhang, H. Yan and Q. Zhao, *Chem. Commun.*, 2016, **52**, 12494-12497.
36. Y. Kim, S. Park, Y. H. Lee, J. Jung, S. Yoo and M. H. Lee, *Inorg. Chem.*, 2016, **55**, 909-917.
37. L. Böhling, A. Brockhinke, J. Kahlert, L. Weber, R. A. Harder, D. S. Yufit, J. A. K. Howard, J. A. H. MacBride and M. A. Fox, *Eur. J. Inorg. Chem.*, 2016, **2016**, 403-412.
38. B. H. Choi, J. H. Lee, H. Hwang, K. M. Lee and M. H. Park, *Organometallics*, 2016, **35**, 1771-1777.
39. R. Furue, T. Nishimoto, I. S. Park, J. Lee and T. Yasuda, *Angew. Chem. Int. Ed.*, 2016, **55**, 7171-7175.
40. J. Kahlert, L. Bohling, A. Brockhinke, H.-G. Stammler, B. Neumann, L. M. Rendina, P. J. Low, L. Weber and M. A. Fox, *Dalton Trans.*, 2015, **44**, 9766-9781.
41. Y. H. Lee, J. Park, S.-J. Jo, M. Kim, J. Lee, S. U. Lee and M. H. Lee, *Chem. Eur. J.*, 2015, **21**, 2052-2061.
42. S.-Y. Kim, A.-R. Lee, Y.-J. Cho, H.-J. Son, W.-S. Han and S. O. Kang, *J. Organomet. Chem.*, 2015, **798**, 245-251.
43. S.-Y. Kim, Y.-J. Cho, G. F. Jin, W.-S. Han, H.-J. Son, D. W. Cho and S. O. Kang, *Phys. Chem. Chem. Phys.*, 2015, **17**, 15679-15682.
44. M. Uebe, A. Ito, Y. Kameoka, T. Sato and K. Tanaka, *Chem. Phys. Lett.*, 2015, **633**, 190-194.
45. H. J. Bae, J. Chung, H. Kim, J. Park, K. M. Lee, T.-W. Koh, Y. S. Lee, S. Yoo, Y. Do and M. H. Lee, *Inorg. Chem.*, 2014, **53**, 128-138.
46. M. Tominaga, H. Naito, Y. Morisaki and Y. Chujo, *New J. Chem.*, 2014, **38**, 5686-5690.
47. S. Kwon, K.-R. Wee, Y.-J. Cho and S. O. Kang, *Chem. Eur. J.*, 2014, **20**, 5953-5960.
48. H. J. Bae, H. Kim, K. M. Lee, T. Kim, Y. S. Lee, Y. Do and M. H. Lee, *Dalton Trans.*, 2014, **43**, 4978-4985.
49. T. Kim, H. Kim, K. M. Lee, Y. S. Lee and M. H. Lee, *Inorg. Chem.*, 2013, **52**, 160-168.
50. L. Weber, J. Kahlert, R. Brockhinke, L. Bohling, J. Halama, A. Brockhinke, H.-G. Stammler, B. Neumann, C. Nervi, R. A. Harder and M. A. Fox, *Dalton Trans.*, 2013, **42**, 10982-10996.
51. K.-R. Wee, Y.-J. Cho, J. K. Song and S. O. Kang, *Angew. Chem. Int. Ed.*, 2013, **52**, 9682-9685.
52. L. Weber, J. Kahlert, L. Bohling, A. Brockhinke, H.-G. Stammler, B. Neumann, R. A. Harder, P. J. Low and M. A. Fox, *Dalton Trans.*, 2013, **42**, 2266-2281.
53. L. Zhu, W. Lv, S. Liu, H. Yan, Q. Zhao and W. Huang, *Chem. Commun.*, 2013, **49**, 10638-10640.
54. K.-R. Wee, Y.-J. Cho, S. Jeong, S. Kwon, J.-D. Lee, I.-H. Suh and S. O. Kang, *J. Am. Chem. Soc.*, 2012, **134**, 17982-17990.
55. J. J. Peterson, A. R. Davis, M. Werre, E. B. Coughlin and K. R. Carter, *ACS Appl. Mater. Interfaces*, 2011, **3**, 1796-1799.
56. B. P. Dash, R. Satapathy, E. R. Gaillard, J. A. Maguire and N. S. Hosmane, *J. Am. Chem. Soc.*, 2010, **132**, 6578-6587.
57. B. P. Dash, R. Satapathy, E. R. Gaillard, K. M. Norton, J. A. Maguire, N. Chug and N. S. Hosmane, *Inorg. Chem.*, 2011, **50**, 5485-5493.
58. M. Tominaga, H. Naito, Y. Morisaki and Y. Chujo, *Asian J. Org. Chem.*, 2014, **3**, 624-631.
59. H. Naito, Y. Morisaki and Y. Chujo, *Angew. Chem.*, 2015, **127**, 5173-5176.
60. T. Kim, J. Lee, S. U. Lee and M. H. Lee, *Organometallics*, 2015, **34**, 3455-3458.
61. H. J. Bae, H. Kim, K. M. Lee, T. Kim, M. Eo, Y. S. Lee, Y. Do and M. H. Lee, *Dalton Trans.*, 2013, **42**, 8549-8552.
62. K. Tanaka, K. Nishino, S. Ito, H. Yamane, K. Suenaga, K. Hashimoto and Y. Chujo, *Faraday Discuss.*, 2017, **196**, 31-42.

63. H. Naito, K. Nishino, Y. Morisaki, K. Tanaka and Y. Chujo, *Chem. - Asian J.*, 2017, **12**, 2134-2138.
64. K. Nishino, K. Uemura, M. Gon, K. Tanaka and Y. Chujo, *Molecules*, 2017, **22**, 2009.
65. J. Cabrera-González, S. Bhattacharyya, B. Milián-Medina, F. Teixidor, N. Farfán, R. Arcos-Ramos, V. Vargas-Reyes, J. Gierschner and R. Núñez, *Eur. J. Inorg. Chem.*, 2017, **2017**, 4575-4580.
66. A. Ferrer-Ugalde, J. Cabrera-González, E. J. Juárez-Pérez, F. Teixidor, E. Pérez-Inestrosa, J. M. Montenegro, R. Sillanpää, M. Haukka and R. Núñez, *Dalton Trans.*, 2017, **46**, 2091-2104.
67. J. Cabrera-González, C. Viñas, M. Haukka, S. Bhattacharyya, J. Gierschner and R. Núñez, *Chem. Eur. J.*, 2016, **22**, 13588-13598.
68. A. Ferrer-Ugalde, A. González-Campo, C. Viñas, J. Rodríguez-Romero, R. Santillan, N. Farfán, R. Sillanpää, A. Sousa-Pedrares, R. Núñez and F. Teixidor, *Chem. Eur. J.*, 2014, **20**, 9940-9951.
69. A. Ferrer-Ugalde, E. J. Juárez-Pérez, F. Teixidor, C. Viñas, R. Sillanpää, E. Pérez-Inestrosa and R. Núñez, *Chem. Eur. J.*, 2012, **18**, 544-553.
70. M. Yoshizawa and J. K. Klosterman, *Chem. Soc. Rev.*, 2014, **43**, 1885-1898.
71. M. Chen, L. Yan, Y. Zhao, I. Murtaza, H. Meng and W. Huang, *J. Mater. Chem. C*, 2018, **6**, 7416-7444.
72. N. Hirofumi, M. Yasuhiro and C. Yoshiki, *Angew. Chem. Int. Ed.*, 2015, **54**, 5084-5087.
73. N. Hirofumi, N. Kenta, M. Yasuhiro, T. Kazuo and C. Yoshiki, *Angew. Chem. Int. Ed.*, 2017, **56**, 254-259.
74. X. Wu, J. Guo, Y. Quan, W. Jia, D. Jia, Y. Chen and Z. Xie, *J. Mater. Chem. C*, 2018, **6**, 4140-4149.
75. H. Naito, K. Nishino, Y. Morisaki, K. Tanaka and Y. Chujo, *J. Mater. Chem. C*, 2017, **5**, 10047-10054.
76. J. Cabrera-González, C. Viñas, M. Haukka, S. Bhattacharyya, G. J. and N. R., *Chem. Eur. J.*, 2016, **22**, 13588-13598.
77. J. He, B. Xu, F. Chen, H. Xia, K. Li, L. Ye and W. Tian, *J. Phys. Chem. C*, 2009, **113**, 9892-9899.
78. J. Gierschner and S. Y. Park, *J. Mater. Chem. C*, 2013, **1**, 5818-5832.
79. J. Gierschner, L. Lüer, B. Milián-Medina, D. Oelkrug and H.-J. Egelhaaf, *J. Phys. Chem. Lett.*, 2013, **4**, 2686-2697.
80. A. R. Popescu, A. D. Musteti, A. Ferrer-Ugalde, C. Viñas, R. Núñez and F. Teixidor, *Chem. Eur. J.*, 2012, **18**, 3174-3184.
81. M. A. Fox, PhD Thesis, University of Durham, 1991.
82. G. Barberà, PhD Thesis Universitat Autònoma de Barcelona, 2002.
83. P. A. V., T. Francesc, S. Reijo, K. Raikko, A. Massimiliano, B. Gemma and V. Clara, *Chem. Eur. J.*, 2009, **15**, 9755-9763.
84. M. Y. Tsang, C. Viñas, F. Teixidor, J. G. Planas, N. Conde, R. SanMartin, M. T. Herrero, E. Domínguez, A. Lledós, P. Vidossich and D. Choquesillo-Lazarte, *Inorg. Chem.*, 2014, **53**, 9284-9295.
85. F. Di Salvo, C. Paterakis, M. Y. Tsang, Y. García, C. Viñas, F. Teixidor, J. Giner Planas, M. E. Light, M. B. Hursthouse and D. Choquesillo-Lazarte, *Cryst. Growth Des.*, 2013, **13**, 1473-1484.
86. W. R. Dawson and M. W. Windsor, *J. Phys. Chem. B*, 1968, **72**, 3251-3260.
87. M. Chaari, J. Cabrera-González, Z. Kelemen, C. Viñas, A. Ferrer-Ugalde, D. Choquesillo-Lazarte, A. Ben Salah, F. Teixidor and R. Núñez, *J. Organomet. Chem.*, 2018, **865**, 206-213.
88. D.-E. Wu, M.-N. Wang, Y.-H. Luo, Y.-W. Zhang, Y.-H. Ma and B.-W. Sun, *New J. Chem.*, 2017, **41**, 4220-4233.
89. R. Davis, N. S. Saleesh Kumar, S. Abraham, C. H. Suresh, N. P. Rath, N. Tamaoki and S. Das, *J. Phys. Chem. C*, 2008, **112**, 2137-2146.
90. D. Gebauer, M. Kellermeier, J. D. Gale, L. Bergstrom and H. Colfen, *Chem. Soc. Rev.*, 2014, **43**, 2348-2371.
91. J. J. M. M. J. Turner, S. K. Wolff, D. J. Grimwood, P. R. Spackman, D. Jayatilaka and M. A. Spackman, CrystalExplorer17, 2017.
92. M. A. Spackman and J. J. McKinnon, *CrystEngComm*, 2002, **4**, 378-392.

93. F. Di Salvo, B. Camargo, Y. Garcia, F. Teixidor, C. Viñas, J. G. Planas, M. E. Light and M. B. Hursthouse, *CrystEngComm*, 2011, **13**, 5788-5806.
94. Z. Wang, T. Wang, C. Zhang and M. G. Humphrey, *Phys. Chem. Chem. Phys.*, 2017, **19**, 12928-12935.
95. A. M. Brouwer, *Pure Appl. Chem.*, 2011, **83**, 2213-2228.
96. G. Sheldrick, *Acta Crystallogr., Sect. A*, 2008, **64**, 112-122.
97. C. F. Macrae, I. J. Bruno, J. A. Chisholm, P. R. Edgington, P. McCabe, E. Pidcock, L. Rodriguez-Monge, R. Taylor, J. van de Streek and P. A. Wood, *J. Appl. Crystallogr.*, 2008, **41**, 466-470.